Solitonic lattice and Yukawa forces in the rare-earth orthoferrite TbFeO3

Artyukhin, Sergey ; Mostovoy, Maxim ; Jensen, N.P.; Le, Duc; Prokes, K.; de paula, V.G.; Nunes Bordallo, Heloisa; Maljuk, A.; Landsgesell, S.; Ryll, H.; Klemke, B.; Paeckel, S.; Kiefer, K.; Lefmann, Kim; Kuhn, Luise T.; Argyriou, D.N.

Published in:
Nature Materials

DOI:
10.1038/nmat3358

Publication date:
2012

Document Version
Publisher's PDF, also known as Version of record

nature materials

ARTICLES

PUBLISHED ONLINE: 24 JUNE 2012 | DOI: 10.1038/NMAT3358

Solitonic lattice and Yukawa forces in the rare-earth orthoferrite $TbFeO_3$

Sergey Artyukhin[1], Maxim Mostovoy[1], Niels Paduraru Jensen[2], Duc Le[3], Karel Prokes[3], Vinícius G. de Paula[3,4], Heloisa N. Bordallo[3,5], Andrey Maljuk[3,7], Sven Landsgesell[3], Hanjo Ryll[3], Bastian Klemke[3], Sebastian Paeckel[3], Klaus Kiefer[3], Kim Lefmann[5], Luise Theil Kuhn[2] and Dimitri N. Argyriou[3,6,8]*

The random fluctuations of spins give rise to many interesting physical phenomena, such as the 'order-from-disorder' arising in frustrated magnets and unconventional Cooper pairing in magnetic superconductors. Here we show that the exchange of spin waves between extended topological defects, such as domain walls, can result in novel magnetic states. We report the discovery of an unusual incommensurate phase in the orthoferrite $TbFeO_3$ using neutron diffraction under an applied magnetic field. The magnetic modulation has a very long period of 340 Å at 3 K and exhibits an anomalously large number of higher-order harmonics. These domain walls are formed by Ising-like Tb spins. They interact by exchanging magnons propagating through the Fe magnetic sublattice. The resulting force between the domain walls has a rather long range that determines the period of the incommensurate state and is analogous to the pion-mediated Yukawa interaction between protons and neutrons in nuclei.

Materials with magnetic transition metal and rare-earth ions show a variety of spectacular effects originating from the coupling between the two spin subsystems. The transition metal spins interact stronger and order at higher temperatures than the spins of rare-earth ions, but they are also much less anisotropic. That is why their orientation can be controlled by the rare-earth magnetism. Such re-orientation transitions observed in many rare-earth ferrites, chromites and manganites have profound effects on their magnetic, optical and elastic properties[1–3].

Recently it was realized that interactions between transition metal and rare-earth spins also play an important role in multiferroic and magnetoelectric materials[4–7]. Thus the coupling between the Mn spins forming a spiral state in the multiferroic $TbMnO_3$ and the Ising-like Tb spins leads to a significant enhancement of the electric polarization induced by the spiral[8,9]. In $GdFeO_3$ orthoferrite the polarization only appears when the independent magnetic orders of Fe and Gd sublattices are present simultaneously[7], whilst in $DyFeO_3$ the interplay between the spins of Fe and Dy ions gives rise to one of the strongest linear magnetoelectric responses observed in single-phase materials[10].

$TbFeO_3$ is an orthorhombic perovskite (space group P*bnm*) where Fe spins order antiferromagnetically in what is called G-type order[11] along the *a* axis and ferromagnetically (F-type) along the *c* axis, as shown in Fig. 1c. This type of commensurate spin order, denoted as G_xF_z, has an onset at approximately $T_N(\mathrm{Fe}) = 650$ K. On cooling in zero field $TbFeO_3$ undergoes two transitions driven by Tb–Tb and Tb–Fe interactions[12,13]. The ordering of Tb spins at $T_N(\mathrm{Tb})\sim 8.5$ K occurs simultaneously with a rotation of Fe spins in the *ac* plane, so that below 8.5 K ferromagnetic components of both Fe and Tb spins align along the *a* axis, whereas their antiferromagnetic components are orthogonal to each other. The magnetic configuration of this intermediate-temperature (IT) phase is F_xG_z for Fe, and $F'_xC'_y$ for Tb (Fig. 1b). However, below ~3 K there is an further spin re-orientation transition to a low-temperature (LT) phase which flips the Fe spins back to their higher temperature G_xF_z order, while the Tb spins order antiferromagnetically in the $A'_xG'_y$ state (Fig. 1a).

Using single-crystal neutron diffraction we have probed the A,C,G and F-type orders in $TbFeO_3$ by tracking the intensity of the corresponding magnetic Bragg reflections in zero field and in an applied field along the *c* axis (see Methods for experimental details). In zero magnetic field our results are consistent with the previously observed sequence of the re-orientation and inverse re-orientation transitions[12]. Above ~8.5 K we find only G-type reflections, although the development of ferromagnetic order is evident from the enhanced intensities of lattice Bragg reflections. Below 8.5 K we find G- and C-type reflections, whereas below 3 K only A- and G-type reflections can be discerned.

In an applied magnetic field (H$\|c$) we find a far more complex behaviour. Here we performed a series of field-cooled measurements, while monitoring accessible A- and G-type reflections. In Fig. 2a we show, in the form of a colour plot, the temperature dependence of scans along *k* around the A-type (001) reflection. At high temperatures this reflection is absent, as there is no order of an A-type component for either the Fe or Tb magnetic sublattice, as indicated in Fig. 1. However, on cooling, a series of reflections appears below 3.8 K that seem to merge into a single peak below ~2.8 K. Examination of the wave vector of these

[1]Zernike Institute for Advanced Materials, University of Groningen, Nijenborgh 4, 9747 AG, Groningen, The Netherlands, [2]Department of Energy Conversion and Storage, Danish Technical University, Risø Campus, Frederiksborgvej 399, DK-4000 Roskilde, Denmark, [3]Helmholtz–Zentrum Berlin für Materialien und Energie, Hahn-Meitner Platz 1, D-14109 Berlin, Germany, [4]Instituto de Física, Universidade do Estado do Rio de Janeiro, Rio de Janeiro, RJ 20559-900, Brazil, [5]Niels Bohr Institute, University of Copenhagen, DK-2100 Copenhagen, Denmark, [6]European Spallation Source ESS AB, PO Box 176, SE-221 00 Lund, Sweden, [7]Leibniz Institute for Solid State and Materials Research Dresden, Helmholtzstrasse 20, 01069 Dresden, Germany, [8]Department of Synchrotron Radiation Research, Lund University, Box 118, Lund, Sweden. *e-mail: dimitri.argyriou@esss.se.

T (K)	$T < 3$ K			3 K < T < 8.5 K			8.5 K < T < 650 K		
Fe	$G_x = 5\mu_B$ $F_z = 0.15\mu_B$	ξ_1	Γ_4	$G_z = 5\mu_B$ $F_x = 0.15\mu_B$	ξ_2	Γ_2	$G_x = 5\mu_B$ $F_z = 0.15\mu_B$	ξ_1	Γ_4
Tb	$A'_x = 6.5\mu_B$ $G'_y = 5\mu_B$	η_1	Γ_8	$F'_x = 2.6\mu_B$ $C'_y = 1.8\mu_B$	η_2	Γ_2			

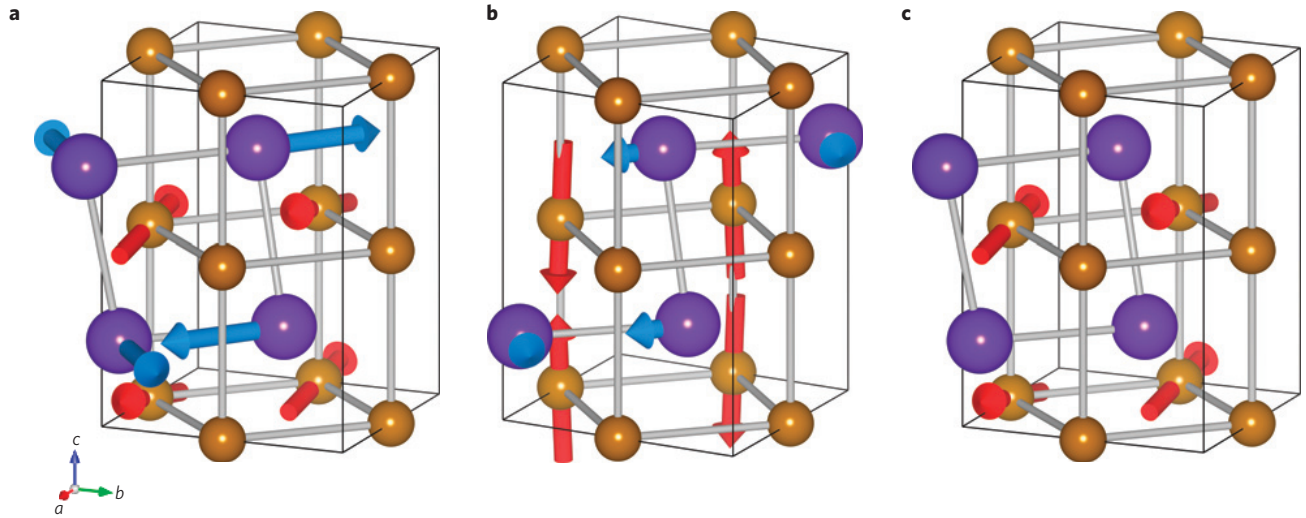

Figure 1 | Uniform magnetic phases of $TbFeO_3$. a–c, The LT phase (**a**), the IT phase (**b**) and the HT phase (**c**). Brown and blue spheres indicate the location of the Fe^{3+} and Tb^{3+} ions, respectively. Red and blue arrows show the average magnetic moments of the ions. Also shown are the corresponding order parameters, irreducible representations and experimental values of magnetic moments[12]. The various types of magnetic order depicted here are labelled as F for a ferromagnetic ordering, G for a the two-sublattice antiferromagnetic Néel state, A for ferromagnetic *ab* planes stacked antiferromagnetically and finally C for ferromagnetic chains parallel to the *c* axis coupled antiferromagnetically.

reflections easily establishes that they are odd harmonics up to 11th order. The wave vector of the first harmonic is $\mathbf{Q} = (0, \epsilon, 1)$, with $\epsilon \sim 0.015$ r.l.u. (Fig. 2b). The incommensurate periodicity of this phase, which we shall refer to as IC, is approximately 67 units cells or ~340 Å. The full width at half maximum of these reflections is relatively sharp, giving a coherence length of ~700 Å or approximately two full cycles of this unusual order. The transition into the IC phase from below is of first order, exhibiting a ~0.2 K hysteresis measured by tracking the intensity of the (0,0,1) reflection, whereas the transition between the IC and the IT phase does not exhibit any hysteresis, as shown by similarly tracking the intensity of the first harmonic reflection (Supplementary Fig. S1).

The physical significance of these observations is that the Tb-spin order in a H‖*c* field develops a square-wave modulation—a periodic array of widely separated domain walls in Tb magnetic order. We ascribe the observed scattering to be dominated by Tb spins; first because of its substantially greater intensity compared to the higher temperature Fe order found around, for example G-type reflections, and also because in zero field A-type reflections are associated only with Tb spin order. In the modulated A-state, Tb spins form ferromagnetic stripes in the *ab* planes with the width 170 Å along the *b* axis. The *a* component of the magnetization alternates from stripe to stripe, whereas the stacking of spins along the *c* axis is antiferromagnetic. Investigation of an Fe G-type reflection under the same condition suggests that Fe spins are weakly perturbed by this unusual Tb order (see Supplementary Information).

On cooling below 2.8 K, Fig. 2a would seem to indicate that the Tb modulation abruptly disappears and the Tb subsystem returns to the zero-field state with the uniform $A'_xG'_y$ order. However, closer inspection of the diffraction data indicates that the (001) reflection on cooling does not yield a simple Gaussian peak shape but rather a Lorentzian, as confirmed by fits to the data. Below, we argue that the Lorentzian peak shape below 2.8 K (Fig. 2c) is indicative of a domain wall disordered phase, which we refer to as LT′.

We have performed measurements similar to those shown in Fig. 2a at various fields as well as two zero-field-cooled measurements at 3.0 and 3.3 K where the field was subsequently applied isothermally to map out the various transitions that occur in this lower temperature regime in $TbFeO_3$. Furthermore, we have conducted capacitance and loss measurements between 0.3 and 10 K in a magnetic field (H‖*c*) between 0 and 1.9 T. The transitions that are evident in the neutron data are correlated with anomalies in both the capacitance and loss data (see Supplementary Information), allowing us to construct the phase diagram shown in Fig. 3. Interestingly, the capacitance and loss data imply that if the sample is cooled in zero field below ~3 K and then field is applied, the transition into the LT′ phase is not reversible and this state can then be stabilized in zero field (Supplementary Fig. S5).

Next we discuss the nature of interactions stabilizing such an unusual periodic domain wall array and holding the domain walls at large distances from each other. Well below $T_N(\mathrm{Fe}) \sim 650$ K the magnitude of the ordered antiferromagnetic moment of the Fe subsystem is independent of temperature, whereas its direction in the *ac* plane described by the angle θ can vary significantly owing to the low magnetic anisotropy of the Fe^{3+} ions. In our notations $\xi_1 = \cos\theta$ is the order parameter of the G_x state, while $\xi_2 = \sin\theta$ describes the G_z ordering. The free energy density of the Fe subsystem is

$$f_{\mathrm{Fe}} = \frac{c}{2}\left(\frac{\mathrm{d}\theta}{\mathrm{d}y}\right)^2 + \frac{K}{2}\sin^2\theta - h\cos\theta \qquad (1)$$

where the first term describes the exchange between Fe spins along the *b* axis, the second term is the magnetic anisotropy, which for

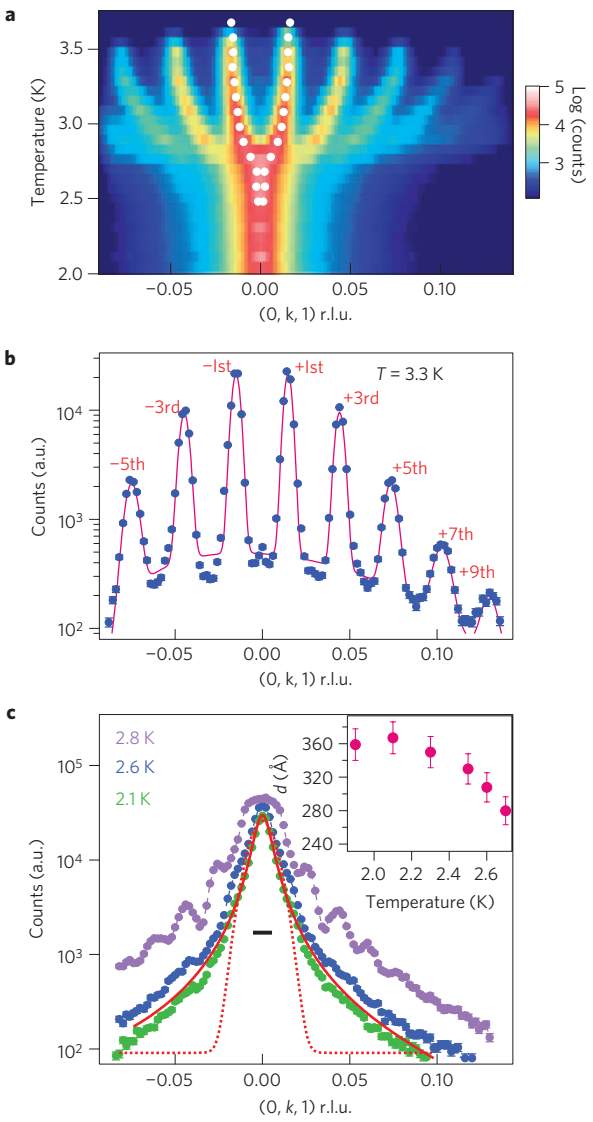

Figure 2 | Single-crystal neutron diffraction data. The measurements were taken on cooling and in a magnetic field parallel to the *c* axis of H||*c* = 2 T. All scans are measured in reciprocal space along (0, *k*,1). In all panels except for the inset in **c**, the data is plotted on a logarithmic scale to show the weaker higher harmonic reflections. **a**, Temperature-dependent neutron diffraction measurements are represented in a two-dimensional plot with intensity depicted as colour on a log scale shown on the right of the panel. White circles are positions of the first harmonic reflection computed by fitting the diffraction data at each temperature to Gaussian peak profiles. **b**, The scan measured at 3.3 K is plotted with the various harmonic reflections labelled accordingly. The data are shown as circles and the continuous line is a fit of a series of Gaussian profiles to the data. **c**, Scans measured at 2.8, 2.6 and 2.1 K show the transition from the IC phase as ϵ rapidly decreases into the LT′ phase. At 2.8 K the various higher harmonic reflections are clearly still evident, whereas at lower temperatures they merge closer together and seem to become almost a single peak. At 2.1 K we find that this diffraction peak is best modelled by a single Lorentzian peak, shown as a red continuous line through the 2.1 K. A single Gaussian peak is shown as a dotted line for comparison and the horizontal black bar represents the resolution of the instrument. The width of the Lorentzian line shape is interpreted as the average distance *d* between neighbouring domain walls (see text). The temperature dependence of *d* determined by modelling the lower temperature data by a single Lorentzian peak is shown in the inset of **c**. Here error bars depict the uncertainty in *d* computed from the least square fit to the data.

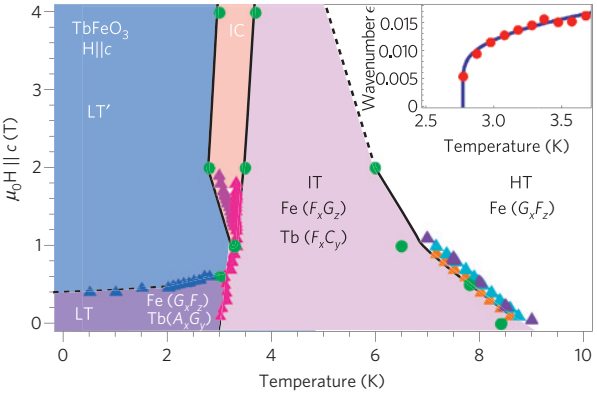

Figure 3 | Magnetic phase diagram of $TbFeO_3$. The phase diagram was determined from neutron diffraction data (shown as circles) and capacitance and loss measurements (shown as triangles), which are described in the Supplementary Figs S2–S5). In the inset we show the temperature dependence of the modulation wave vector ϵ measured in an applied magnetic field $\mu_0 H_c = 2$ T. The blue line is the fit obtained using the theoretical description of the IC state in terms of the periodic kink array.

$K > 0$ favours the G_x order, and the last term is the Zeeman interaction with the magnetic field H_z in the G_xF_z state.

The free energy of Tb spins is expanded in powers of the order parameters η_1, describing the zero-phase LT state with antiparallel Tb spins in neighbouring *ab* layers (Fig. 1a), and η_2, describing the IT state with parallel Tb spins in neighbouring layers (Fig. 1b):

$$f_{\mathrm{Tb}} = \frac{c_1}{2}\left(\frac{\mathrm{d}\eta_1}{\mathrm{d}y}\right)^2 + \frac{c_2}{2}\left(\frac{\mathrm{d}\eta_2}{\mathrm{d}y}\right)^2 + \frac{a_1}{2}\eta_1^2 + \frac{a_2}{2}\eta_2^2 + \frac{b_1}{4}\eta_1^4 + \frac{b_{12}}{2}\eta_1^2\eta_2^2 + \frac{b_2}{4}\eta_2^4 + \cdots \quad (2)$$

For $\Delta = a_2 - a_1 > 0$ the Tb subsystem would order in the state with $\eta_1 \neq 0$ below some temperature T_0, at which $a_1 = 0$. However, the interaction between the Tb and Fe spins favours the IT state with $\eta_2 \neq 0$ and $\theta = \pm\pi/2$, in which both subsystems have a ferromagnetic moment along the *a* axis. Because η_2 and $\xi_2 = \sin\theta$ transform in the same way (see Supplementary Information), this interaction is a linear coupling,

$$f_{\mathrm{Fe-Tb}} = -\lambda\xi_2\eta_2 \quad (3)$$

For $\lambda^2 > \Delta K$ the 'unnatural' IT state, with parallel Tb spins in neighbouring layers and Fe spins rotated by 90° away from the easy axis, intervenes between the states with the 'natural' orders of Fe and Tb spins. In this way one obtains the zero-field phase diagram of $TbFeO_3$ (refs 12,14).

Symmetry of $TbFeO_3$ also allows for two Lifshitz invariants linear in order parameter gradients,

$$f_{\mathrm{L}} = g_1\left(\eta_1\partial_y\xi_2 - \xi_2\partial_y\eta_1\right) + g_2\left(\eta_1\partial_y\eta_2 - \eta_2\partial_y\eta_1\right) \quad (4)$$

which favour the experimentally observed periodic spin modulation along the *b* axis. The first and the second invariants originate, respectively, from the Tb–Fe and Tb–Tb interactions. Similar terms inducing modulations along the *a* and *c* axes are forbidden by symmetry. Minimizing the total free energy—the sum of equations (1) through to (4)—we obtain the phase diagram shown in Fig. 4a, which includes a narrow incommensurate phase region, which we identify with the IC phase revealed in our neutron data.

It is important to stress the difference between the IC state in $TbFeO_3$ and the long-period spin spirals in non-centrosymmetric

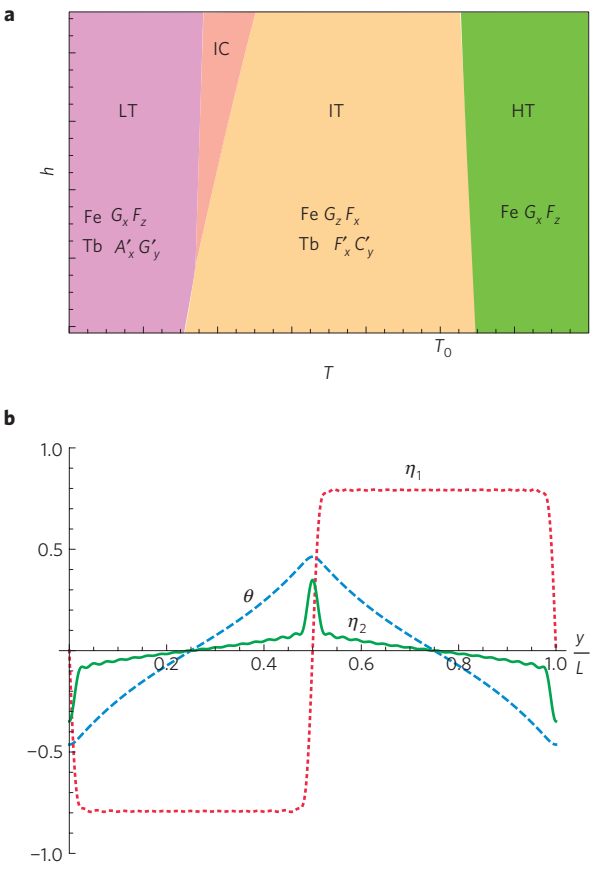

Figure 4 | Theoretical phase diagram and the structure of the IC state. **a**, Magnetic phase diagram of the Landau model of $TbFeO_3$ including the Fe–Tb interaction described by the first Lifshitz invariant in equation (4). The parameters used to obtain this phase diagram are: $\Delta = 0.5$, $K = 0.125$, $\lambda = 0.275$, $b_1 = b_2 = 1.0$, $b_{12} = 2.4$, $g_1 = 0.187$, $g_2 = 0$, $c = 1$ and $c_1 = c_2 = 0.01$. **b**, The y-dependence of the Tb order parameters, η_1 (red line) and η_2 (green), and the angle θ measured in radians (blue) describing the fan-like rotation of Fe spins in the IC state with the period $L = 340$ Å.

magnets, also described using Lifshitz invariants[15]. First, the crystal lattice of $TbFeO_3$ is centrosymmetric (inversion symmetry is only broken in the LT phase by the Tb spin ordering). Equation (4) is the interaction between two distinct magnetic phases: the LT Tb state (odd under inversion) and the IT phase (even under inversion). It is only effective close to the boundary where these two phases have equal free energies, which is why the IC state is observed in a very narrow region of the phase diagram.

Second, spirals in non-centrosymmetric magnets result from the relatively weak spin–orbit coupling[15,16]. On the other hand, the coupling equation (4) may originate from a stronger Heisenberg exchange: in the Supplementary Information we give symmetry arguments showing that the exchange interactions between the Tb and Fe spin orders varying along the b axis do not cancel. Furthermore, the coupling between two Tb order parameters (the second term in equation (4)) resulting from interactions between rare-earth spins separated by relatively long distances, is expected to be much weaker than interactions between the Tb and Fe spins described by the first term (in our calculations $g_2 = 0$).

Third and most important, the observation of the large number of Fourier harmonics in the IC state of $TbFeO_3$ shows that this state is qualitatively different from a magnetic spiral with slowly varying spin vectors. To account for the difference between the isotropic Fe spins and the Ising-like Tb spins[13,17], we assumed that $c_1, c_2 \ll c$ and allowed for 40 harmonics in the periodic modulation of order parameters when we minimized the free energy. The resulting incommensurate state is shown in Fig. 4b. Whereas the angle θ describing the Fe spins undergoes small amplitude fan-like oscillations around zero, corresponding to the oscillations of the weak ferromagnetic moment of Fe ions around the applied magnetic field $H \| c$, the low-temperature Tb order parameter η_1 exhibits sudden jumps.

To understand the nature of the force that holds these atomically sharp domain walls at distances of ~170 Å from each other, we (briefly) discuss an interesting field-theoretical interpretation of the coupled system of rare-earth and transition metal spins. Consider a single domain wall located at $y = 0$ where the Ising-like LT order parameter η_1 shows a discontinuous jump from $-|\eta_1|$ to $+|\eta_1|$ or vice versa (Fig. 5a). Such a kink can be assigned the topological charge $Q = (\eta_1(+\infty) - \eta_1(-\infty))/2|\eta_1| = \pm 1$. The free energy per unit area of the domain wall is the 'bare' energy $F_{DW}^{(0)}$ resulting from interactions between Tb spins plus

$$F_\theta = -2g\theta(0)Q + \frac{1}{2}\int \mathrm{d}y \left[c\left(\frac{\mathrm{d}\theta}{\mathrm{d}y}\right)^2 + (K+h)\theta^2 \right] \qquad (5)$$

where the first term is the Lifshitz invariant equation (4) ($g = 2g_1|\eta_1|$ and $g_2 = 0$), describing the interaction between the Tb and Fe spins, while the second term is the free energy of Fe spins for $|\theta| \ll 1$. Equation (5) can be interpreted as an energy of a charged plane with the surface charge density gQ interacting with the field θ, which describes spin waves in the Fe magnetic subsystem. Minimizing F_θ with respect to $\theta(y)$, we obtain the distortion in the Fe spin ordering produced by the Tb domain wall, $\theta(y) = (Qg/\sqrt{c(K+h)})\mathrm{e}^{-(|y|/l)}$ (Fig. 5a), which reduces the domain wall free energy:

$$F_{DW} = F_{DW}^{(0)} - \frac{g^2}{\sqrt{c(K+h)}} \qquad (6)$$

When F_{DW} becomes negative, the domain walls tend to condense. Their density is, however, limited by the effective long-range repulsion between the domain walls resulting from the exchange of magnons. This interaction is analogous to the pion-mediated Yukawa force between protons and neutrons in nuclei[18]. The sharp domain walls in the Tb spin subsystem play the role of nucleons, while magnons propagating through the Fe spin subsystem play the role of massive pions. The analogue of the pion mass is a small gap in the magnon spectrum, which limits the range of this interaction by the length $l = \sqrt{c/K+h}$, much larger than the lattice constant. This Yukawa-like force attracts equal 'electric' charges and repels opposite ones. Because the topological charges of domain walls alternate along the b axis, neighbouring domain walls in a periodic array have opposite 'electric' charges, resulting in net repulsion. The interaction between two neighbouring domain walls located at y_1 and y_2 (Fig. 5b) is

$$U(y_2 - y_1) = \frac{g^2}{\sqrt{c(K+h)}}\mathrm{e}^{-\frac{|y_2 - y_1|}{l}} \qquad (7)$$

and the total 'electrostatic' free energy of an array of domain walls with the charges $\{Q_n\}$ alternating along the b axis (including the 'self-energy' of the charged surfaces) is given by

$$F_\theta = -\sum_{n,m} Q_n U(y_n - y_m) Q_m \qquad (8)$$

where y_n is the position of the nth kink. Minimizing the free energy density for an equidistant array of kinks (Fig. 5c), we obtain the optimal period of the incommensurate state. Its temperature dependence fits well the experimental data above 2.8 K, as shown

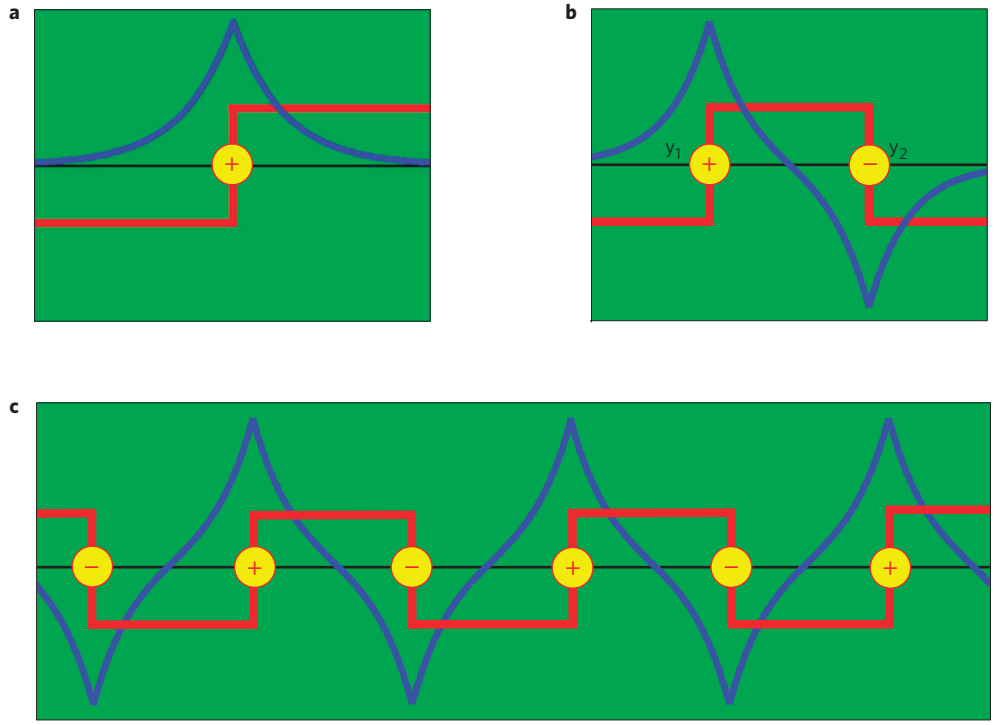

Figure 5 | Topological defects in the coupled orders of Tb and Fe spins. a–c, Domain wall (kink) in Tb ordering (red line) and the angle θ (blue line) describing the perturbation of Fe spins near the domain wall (**a**), kink–antikink pair (**b**) and periodic array of domain walls with alternating charges (**c**).

in the inset of Fig. 3. The length scale for the period of the IC state, set by $l \sim 150$ Å, is essentially the thickness of the domain wall in the antiferromagnetic ordering of Fe spins, even though such walls are not present in the IC state. Thus the long period of the IC state of Tb spins originates from the large stiffness and low magnetic anisotropy of the Fe magnetic subsystem.

So far in our considerations we have not taken into account crystal imperfections, which result in pinning of the domain walls and destruction of the long-range incommensurate ordering. The inset of Fig. 2c shows that the average distance between the Tb domain walls grows as temperature decreases. This weakens the magnon-mediated interactions between the domain walls and increases the role of disorder. For randomly positioned domain walls the correlation function of the A-type Tb order parameter decays exponentially with the distance: $\langle A(y)A(0)\rangle \propto e^{-2|y|/d}$, where d is the average distance between the walls, resulting in a broad A-type reflection with the Lorentzian shape, which fits well our neutron data for $T < 2.8$ K and $\mu_0 H_c > 0.5$ T (Fig. 2c). This explains the origin of the LT′ phase in the experimental phase diagram shown in Fig. 3.

The tantalizing suggestion from our work is that periodic domain wall arrays may be present in other orthoferrites and orthochromites. Lifshitz invariants similar to equation (4) are certainly allowed by symmetry in multiferroic materials, such as $GdFeO_3$, where electric polarization is induced by a transition metal spin order (even under inversion and weakly ferromagnetic) coexisting with a rare-earth spin order odd under inversion[7]. Long-ranged interactions between domain walls in these two orders resulting from such invariants can have a strong effect on switching of the spontaneous electric polarization with an applied magnetic field and vice versa.

Methods

Single crystals of $TbFeO_3$ were grown under an oxygen pressure of 4 bar using the crucible-free floating-zone method. Their quality was checked by X-ray diffraction. Neutron diffraction experiments were carried out on a large single crystal of $TbFeO_3$, at the BER-II reactor of the Helmholtz Zentrum Berlin using the FLEX cold triple-axis spectrometer with collimation of 60′–60′–60′, $k_i = 1.3$ Å^{-1}, and a cooled Be filter positioned in the scattered beam. Further measurements were made also with the E4 two-axis diffractometer with $\lambda = 2.8$ Å. In both cases a magnetic field was applied along the c-axis of the sample using a superconducting horizontal field magnet. Dielectric measurements were performed at the Laboratory for Magnetic Measurements at the Helmholtz–Zentrum Berlin, with temperatures varying between 0.3 K and 15 K and with magnetic fields up to 2 T. Magnetization field and temperature control were provided by an Oxford Instruments 14.5 T cryomagnet equipped with a Heliox ^{3}He insert. An Andeen–Hagerling 2700A Capacitance Bridge was used to measure the capacitance and loss of a disc-shaped sample of $TbFeO_3$, which was mounted between the electrodes of a parallel plate capacitor.

Received 21 March 2011; accepted 15 June 2012; published online 24 June 2012

References

1. Belov, K. P., Zvezdin, A. K., Kadomtseva, A. M. & Levitin, R. Z. Spin-reorientation transitions in rare-earth magnets. *Sov. Phys. Usp.* **19,** 574–596 (1976).
2. Buchel'nikov, V. D., Dan'shin, N. K., Tsymbal, L. T. & Shavrov, V. G. Magnetoacoustics of rare-earth orthoferrites. *Phys. Usp.* **39,** 547–572 (1996).
3. Kimel, A. V. *et al.* Ultrafast non-thermal control of magnetization by instantaneous photomagnetic pulses. *Nature* **435,** 655–657 (2005).
4. Kimura, T. *et al.* Magnetic control of ferroelectric polarization. *Nature* **426,** 55–58 (2003).
5. Hur, N. *et al.* Electric polarization reversal and memory in a multiferroic material induced by magnetic fields. *Nature* **429,** 392–395 (2004).
6. Zvezdin, A. K. & Mukhin, A. A. Magnetoelectric interactions and phase transitions in a new class of multiferroics with improper electric polarization. *JETP Lett.* **88,** 505–510 (2008).
7. Tokunaga, Y. *et al.* Composite domain walls in a multiferroic perovskite ferrite. *Nature Mater.* **8,** 558–562 (2009).
8. Prokhnenko, O. *et al.* Coupling of frustrated ising spins to the magnetic cycloid in multiferroic $TbMnO_3$. *Phys. Rev. Lett.* **99,** 177206 (2007).
9. Aliouane, N. *et al.* Magnetic order and ferroelectricity in $RMnO_3$ multiferroic manganites: Coupling between R- and Mn-spins. *J. Phys. Condens. Matter* **20,** 434215 (2008).
10. Tokunaga, Y., Iguchi, S., Arima, T. & Tokura, Y. Magnetic-field-induced ferroelectric state in $DyFeO_3$. *Phys. Rev. Lett.* **101,** 097205 (2008).
11. Bertaut, E. F. in *Magnetism* Vol. 3 (eds Rado, J. T. & Suhl, H.) 149–209 (Academic, 1963).
12. Bertaut, E. F., Chappert, J., Mareschal, J., Rebouillat, J. P. & Sivardière, J. Structures magnetiques de $TbFeO_3$. *Solid State Commun.* **5,** 293–298 (1967).

13. Bouree, J. E. & Hammann, J. Mise en évidence expérimentale des effets de forme dans l'orthoferrite de terbium. *J. Phys.* **36,** 391–397 (1975).
14. Belov, K. P., Zvezdin, A. K. & Mukhin, A. A. Magnetic phase transitions in terbium orthoferrite. *Sov. Phys. JETP* **49,** 557–562 (1979).
15. Dzyaloshinskii, I. Theory of helical structures in antiferromagnets I: Nonmetals. *Sov. Phys. JETP* **19,** 960–971 (1964).
16. Moriya, T. Anisotropic superexchange interaction and weak ferromagnetism. *Phys. Rev.* **120,** 91–98 (1960).
17. Bidaux, R., Bouree, J. E. & Hammann, J. Dipolar interactions in rare earth orthoferrites—II. *J. Phys Chem. Solids* **36,** 655–659 (1975).
18. Kemmer, N. Nature of the Nuclear Field. *Nature* **141,** 116–117 (1938); http://www.nature.com/physics/looking-back/kemmer/index.html.

Acknowledgements

D.N.A. and S.L. thank the Deutsche Forschung Gemeinschaft for support under contract AR 613/2-1. The neutron scattering work was supported by the Danish National Research Council through DANSCATT. N.P.J. thanks J. B. Hansen, for support and guidance. M.M. was supported by the FOM grant 08.0952.

Author contributions

D.N.A. initiated the project, D.N.A. and M.M. interpreted the results and wrote the paper, and M.M. and S.A. developed the theory. N.P.J. and H.N.B. contributed to the interpretation of the experimental results. K.L. and L.T.K. supported the project. Neutron experiments and analysis of these data were conducted by N.P.J., D.N.A., K.P., D.L., V.G.P. and H.N.B. Bulk property and characterization measurements were conducted by S.L., H.R., B.K., S.P. and K.K., and A.M. grew the single crystal. All authors commented on the manuscript.

Additional information

The authors declare no competing financial interests. Supplementary information accompanies this paper on www.nature.com/naturematerials. Reprints and permissions information is available online at www.nature.com/reprints. Correspondence and requests for materials should be addressed to D.N.A.